

Article

System Design and Mechanism Study of Ultrasonic-Assisted Electrochemical Grinding for Hard and Tough Materials

Chen Hu ^{1,2} and Yongwei Zhu ^{1,*}¹ College of Mechanical Engineering, Yangzhou University, Yangzhou 225127, China; huchen1988040@163.com² Yangzhou Polytechnic Institute, Yangzhou 225127, China

* Correspondence: ywzhu@yzu.edu.cn

Abstract: In this study, an ultrasonic-assisted electrochemical grinding (UAECG) system was designed to improve the low efficiency and tool wear in conventional grinding of hard and tough materials. In this system, multiple-field energy consisting of ultrasonic, electrochemical and mechanical grinding was used. The processing mechanism was investigated to determine the interaction mechanism between ultrasonic, grinding and electrochemical processing. The established theoretical model showed that the processing efficiency was affected by the ultrasonic amplitude, ultrasonic frequency, electrolyte conductivity and other parameters. In verifying the feasibility of UAECG machining and the effect of machining elements on machining, a series of corresponding machining experiments was conducted. Experiments showed that the machining efficiency can be improved by machining through the UAECG system. The material removal rate of W18Cr4V machining was 2.7 times higher than that of conventional grinding and 1.7 times higher than UAG. The processing efficiency of YT15 was increased by 3.2 times when the processing voltage increased from 2 to 6 V. The surface shape and roughness were also affected by these parameters. The surface roughness of the SiCp/Al workpiece reached the best level at 4 V as the machining voltage increased from 2 to 6 V. However, the surface roughness increased significantly when the voltage increased to 6 V. Thus, parameters such as machining voltage must be optimised for efficient and precise machining in practice.

Keywords: rotary ultrasonic machining; compound electrochemical; compound grinding; collaborative machining system



Citation: Hu, C.; Zhu, Y. System Design and Mechanism Study of Ultrasonic-Assisted Electrochemical Grinding for Hard and Tough Materials. *Processes* **2023**, *11*, 1743. <https://doi.org/10.3390/pr11061743>

Academic Editors: Jei-Zheng Wu and Chia-Yu Hsu

Received: 14 May 2023

Revised: 31 May 2023

Accepted: 5 June 2023

Published: 7 June 2023



Copyright: © 2023 by the authors. Licensee MDPI, Basel, Switzerland. This article is an open access article distributed under the terms and conditions of the Creative Commons Attribution (CC BY) license (<https://creativecommons.org/licenses/by/4.0/>).

1. Introduction

In recent years, various hard and tough materials have been widely used for the manufacturing of high-tech equipment in the national defence and aerospace industry, such as high-speed steel (W18Cr4V), cemented carbide (YT15) and silicon carbide particle-reinforced aluminium (SiCp/Al). These materials are characterised by high hardness and toughness [1]. Thus, when traditional mechanical machining methods such as grinding are used, superhard tool materials such as diamonds are required in conventional processing such as grinding. Nevertheless, the tools are severely worn at high cutting forces and temperatures. The workpiece is also prone to bursting, thereby causing surface quality defects [2,3].

Special machining techniques have received special attention, and they are widely used in practice because of their advantages, such as low machining forces and independence from material hardness [4]. However, a single special machining method has its own shortcomings. Ultrasonic machining has low cutting stress and low heat, but the tool electrodes are easily worn and difficult to maintain [5]. Electrochemical machining is more efficient, but it suffers from low machining accuracy [6]. In addressing the defects of single special machining, composite machining has become a hot research topic. In processing

the above-mentioned materials, many scholars have selected ultrasonic-assisted grinding (UAG) and ultrasonic electrochemical processing for their research.

UAG can effectively reduce tool wear at a low grinding force and heat caused by the intermittent cutting effect and hammering effect of ultrasonic vibration. Hard, tough materials fall under high-frequency striking. Given the above-mentioned advantages, scholars have conducted extensive research on UAG. Gao [7] revealed ultrasonic-assisted cutting characteristics based on kinematic modelling and relative motion trajectory simulation. The experiments showed that the surface of the workpiece machined by this machining method exhibited significant widening of the grooves, which were uniformly distributed at approximately 6–8 μm . Therefore, compared with conventional grinding machining (GM), UAG shows evident and unique machining characteristics. Zhang [8] investigated the material removal mechanism in the end face direction and constructed a prediction model for grinding forces during ultrasonic-assisted machining. The experimental results showed that the predicted and measured values of grinding forces were quite close to each other, and the grinding forces were significantly reduced after the introduction of ultrasonic vibration. Shen [9] found that the matching of vibration and milling parameters has an important effect on the final surface topography, and the size of the overlap area of multiple cuts can accurately reflect the surface topography. Li [10] used UAG for the surface machining of silicon carbide-based composites. The kinematics were analysed between individual diamond abrasives and workpiece materials. The mathematical relationship between cutting parameters and vibration parameters was established; meanwhile, the conditions for intermittent machining were obtained. The indentation fracture theory and kinematic analysis were used to establish the cutting force model. The comparison of experimental and simulated data showed that the errors of model and experimental values were less than 15% in most tests. Wang [11] applied elliptical ultrasonic vibration grinding to surface machining to investigate the effect of machining performance and machined surface quality. The impacts of different parameters on machining force, surface roughness and machined surface topography were compared. The test showed that the processing method has significant advantages with regard to surface topography and minimum surface roughness. Zhang [12] conducted a modelling and mechanism study on the grinding force and material removal rate (MRR). Meanwhile, the impacts of processing parameters of ultrasonic vibration on grinding force and surface microstructure were analysed. The test showed that ultrasonic vibration-assisted grinding has an excellent performance in the machining of hard, tough materials.

Ultrasonic electrochemical processing utilises electrochemical action and ultrasonic cavitation. The passivation film produced by electrochemical processing is continuously removed by ultrasonic cavitation, whereas ultrasonic vibratory pumping promotes the flow of electrolyte renewal and accelerates the electrochemical efficiency. Advantages such as ultrasonic and electrochemical action as well as the non-contact processing method can promote the processing of hard, tough materials. Given the above-mentioned technological advantages, scholars have conducted intensive studies. Bhattacharyya [13] designed the processing system, and the MRR and processing accuracy were controlled successfully. Experiments showed that an electrolyte concentration range of 15–20 g/L reduced the stray current effect, and tool vibration improved the ability of the interpole clearance to remove sludge, thereby changing the MRR and accuracy. Ghoshal [14] experimentally analysed the processing effect of machining parameters. The experiments showed that high-quality micro workpieces with different shapes could be produced by varying the electrochemical voltage or by using the appropriate amplitude of vibration. Skoczypiec [15] used the fluid dynamics method to analyse the clearance of electrolyte flow through the electrolyte during ultrasonic vibration-assisted electrochemical machining, obtain the optimal conditions for electrolyte flow and achieve the effect of ultrasonic vibration on the machining through experiments. Wang [16] conducted experiments on stainless-steel microvia using this processing method. Experiments showed that the processing speed, surface quality and maximum depth of the processed microvia are significantly increased,

whereas the taper and diameter are reduced. Wang [17] applied low-frequency sinusoidal oscillatory motion to the workpiece and derived the MRR and the inter-electrode clearance pressure mathematical model. The vibration amplitude and frequency have important effects on processing efficiency and feed rate; thus, a higher MRR can be obtained by applying a larger vibration amplitude and the appropriate frequency.

The efficiency and accuracy of the two above-mentioned composite machining processes have been proven by considerable research. However, few articles have mentioned methods and experiments on the combined processing of ultrasound, mechanical and electrochemical energy. The interactive effects of the coupling of more than three energy fields are also rarely discussed. In optimising the machining method, the two composite machining methods are combined, which is called the ultrasonic-assisted electrochemical grinding (UAECG) system. Three energy field machining methods, namely, ultrasonic, electrochemical and rotary grinding, are used in this system.

In this paper, the structural design and online systems were constructed. The material removal mechanism was theoretically studied on the basis of the system. The experiments were performed using different kinds of materials (W18Cr4V, YT15 and SiCp/Al) and different kinds of parameters (electrolytic voltage). The practical effects of machining on the machining effect and surface morphology were studied. This study has increased the understanding of the relationship between the actions of ultrasonic processing, electrolysis and grinding. The efficiency and accuracy of the combination of the three above-mentioned processing methods were also realized, which indicates its application potential.

The article consists of five parts. This part primarily introduces the background of the thesis research and the significance of the research. The processing principle and the theoretical model of UAECG processing are constructed in Section 2. Equipment, including the rotary ultrasonic grinding processing device, online measurement and control system are shown in Section 3. The materials and methods and steps of the experiments are introduced accordingly. The results of the experiments and a discussion of the results are provided in Section 4. Conclusions are drawn in Section 5.

2. Analytical Modelling

The basic principle of this machining system is shown in Figure 1a. During machining, the tool head is rotated and fed at a constant speed along the Z-axis whilst ultrasonically vibrating along the Z-axis under the action of the ultrasonic device. Simultaneously, the tool electrode is connected to the negative side of the electrochemical power supply, whereas the workpiece is connected to the positive side. The ultrasonic vibration displacement curve of the tool in one cycle is shown in Figure 1b. In this case, electrochemical, ultrasonic and grinding interact with one another.

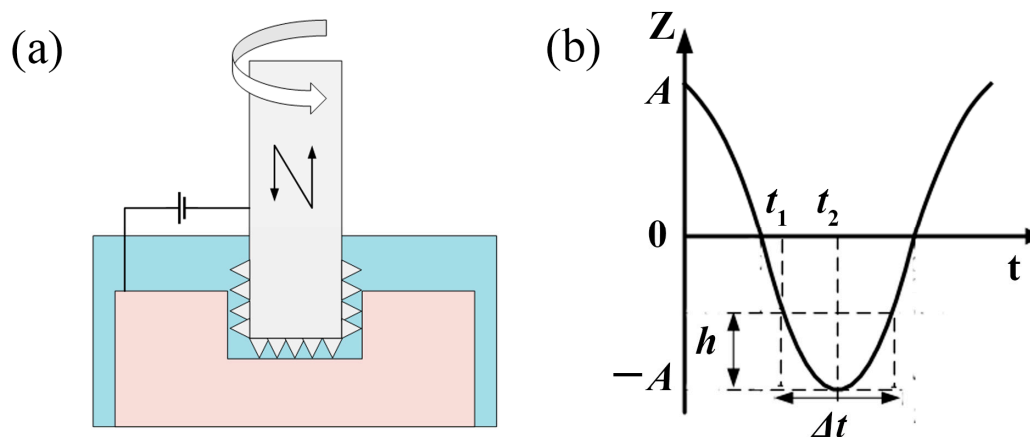


Figure 1. (a) Fundamental principles and (b) tool head displacement curve.

Before the moment t_1 , the system is primarily processed by ultrasonic-assisted electrochemical processing because the workpiece is not in contact with the tool. Based on the anodic dissolution principle, with the tool electrode slowly feeding towards the workpiece, the surface metal of the workpiece is dissolved by the tool electrode [18]. Based on the law of electrochemical machining, anode dissolution tends to form a passivation film on the workpiece surface, which will have a passivation effect during electrochemical processing. [19] Considering that ultrasonic and rotary movements are produced in this system, the abrasives in the electrolyte constantly affect the surface of the workpiece at high frequencies, destroying the anodic passivation film covered on the surface of the workpiece [20]. In addition, the ultrasonic and rotary motion accelerates the electrolyte between the workpiece and the tool electrode, which promotes the evacuation of process debris and heat, thereby enhancing material removal efficiency [21].

After the moment t_1 , the tool electrode continues to move downward. Once the tool grinding head contacts the workpiece, ultrasonic grinding begins. Although electrochemical grinding is also present in this process, the electrochemical speed is slower than the grinding feed. Thus, grinding is the primary process. Considering that grinding becomes intermittent by ultrasonic vibration, the grinding force is reduced; meanwhile, the grinding removal capacity is increased [22].

After the moment t_2 , the tool electrode starts to move slowly upward until it leaves the workpiece, and the total time experienced by grinding is Δt . Thereafter, the processing shifts again from ultrasonic grinding processing to ultrasonic electrochemical processing.

In this system, a synchronous co-electrochemical device was designed to optimise the energy-matching relationship. The basic principle is shown in Figure 2. The tool electrode moves sinusoidally under ultrasonic action, and the clearance between the end face and the workpiece decreases and increases periodically. Considering that the tool electrode is coated with microscopic abrasive particles, a minimum clearance Δ_{\min} is observed. When the clearance is between Δ_{\min} and the set Δ_s , the modulation circuit controls the closure of the chopper switch to perform electrochemical processing for material removal. When the clearance exceeds the set Δ , the modulating circuit controls the chopper switch to open, and the electrochemical processing is stopped, at which time the processing debris is excluded and the working fluid is renewed to prepare for the next stage of electrochemical processing. This device enables the machining process to maintain a small clearance, which improves electrochemical energy utilisation whilst increasing the machining efficiency. The short circuit and direct contact with the electrode and workpiece are avoided because of the existence of the minimum clearance Δ_{\min} caused by tiny abrasive particles.

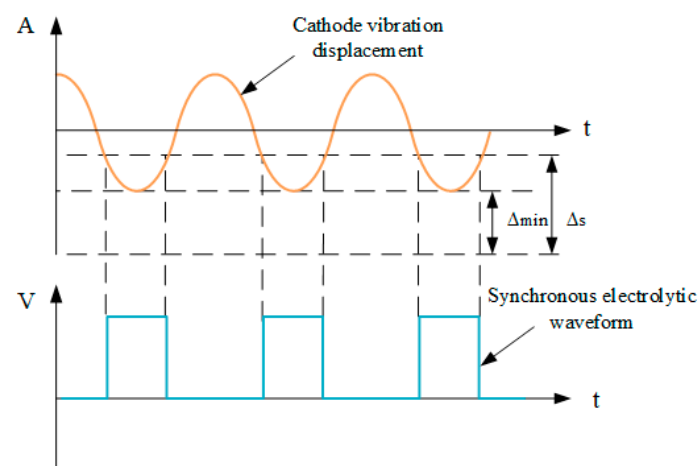


Figure 2. Synchronous processing control principle.

2.1. Modelling of UAG

Plastic removal can significantly reduce surface damage and improve surface quality. Based on the principle of indentation fracture mechanics, determining the critical depth of cut of the abrasive grains for plastic transformation based on the microhardness and fracture toughness of the material is the key to achieving plastic processing [23]. When the maximum depth of penetration of the abrasive grain is less than the critical depth of penetration, plastic removal is the primary removal method [24]. In simplifying the model, the following assumptions are drawn:

- (1) The ultrasonic amplitude, vibration frequency and tool radius are fixed, and the losses in machining are not considered.
- (2) All abrasives are uniformly arranged and distributed in the same plane, and they are considered rigid spheres of equal size, which simultaneously participate in the machining.
- (3) Plastic removal is used as the material removal model.

Based on the moving trajectory of the tool electrode, the motion equation of the abrasive particles can be obtained. The material removal amount of each abrasive particle in the ultrasonic high-frequency vibration cycle can be calculated, and then the total number of abrasive particles in the whole cycle can be derived.

The UAG can be subdivided into the hammering effect of ultrasonic vibration, the abrasive effect of rotary motion and the compound tearing effect of both processes [25]. When the tool rotates at a high speed with the ultrasonic spindle, ultrasonic high-frequency vibration will be carried out along the tool axis simultaneously. The tool will continuously feed in the direction of the workpiece at a fixed speed. The solidified microscopic abrasive particles will continuously affect and polish the workpiece surface to complete the stripping of the material. Intermittent cutting is formed by the combined effect of axial rotational force and ultrasonic high-frequency vibration [26]. This method improves machining efficiency whilst reducing cutting forces and cutting heat, thereby reducing machining losses [27]. The Z-axis trajectory of the tool electrode vibration direction $z(t)$ can be expressed using the following formula:

$$z(t) = A \sin(2\pi ft + \frac{\pi}{2}) \quad (1)$$

where A is the tool electrode amplitude, f is the ultrasonic frequency and t is the processing time.

Based on the electrode motion pattern shown in Figure 1, the contact time between the tool electrode and the workpiece in a single cycle is denoted by Δt [12]:

$$\Delta t = 2(t_2 - t_1) = \frac{1}{\pi f} \left[\frac{\pi}{2} - \arcsin\left(1 - \frac{h}{A}\right) \right] \quad (2)$$

where h is the depth of the abrasive grain into the material.

The radius of the circle of the scanned cross-section on the workpiece surface increases as the microgrits cut deeper. The volume of the material removed by a single microgrind in a single cycle can be approximated as an ellipsoidal defect [8]. Thus, in a single cycle, the material removal depth h_1 machined by the number of microfine sharpening for N can be calculated using the following formula [28]:

$$h_1 = \frac{N\pi^2 n R h^2}{S\pi f \sqrt{2rh - h^2}} \left[\frac{\pi}{2} - \arcsin\left(1 - \frac{h}{A}\right) \right] \left(r - \frac{h}{3} \right) \quad (3)$$

where r is the radius of the grinding grain, R is the distance from the grinding grain to the centre of the tool face, n is the tool electrode speed and S is the machining cross-sectional area.

2.2. Modelling of Ultrasonic-Assisted Electrochemical Processing

According to Faraday's law, when ultrasonic compound electrochemical processing occurs, the total amount of material removed during electrochemical processing, V_a , can be calculated by using the following equation:

$$V_a = D\eta\omega\sigma\frac{U_r}{\Delta} \quad (4)$$

where D is the duty cycle of the electrochemical current, η is the current efficiency, ω is the total volume electrochemical equivalent of the material being electrolysed, σ is the electrolyte conductivity, U_r is the voltage in the interstitial electrolyte and Δ is the electrolyte processing clearance.

As shown in Figure 2, the ultrasonic compound pulse electrochemical clearance varies periodically because of the introduction of the synchronous ultrasonic device [29]. The electrochemical depth h_2 of a single cycle can be expressed by using the following equation:

$$h_2 = \int_{t_3}^{t_4} v_a(t)dt \quad (5)$$

The actual electrochemical time in a single cycle can be expressed by using the following equation:

$$\Delta t = (t_4 - t_3) = \frac{1}{\pi f} \left[\frac{\pi}{2} - \arcsin\left(1 - \frac{\Delta_s - \Delta_{\min}}{A}\right) \right] \quad (6)$$

Considering that the minimum spacing Δ_{\min} determined by the abrasive diameter being larger than the ultrasonic amplitude A , the machining clearance of Δt can be expressed by the average clearance between Δ_{\min} and Δ_s . Thus, equation (9) can be approximated by using the following equation:

$$h_2 = \int_{t_3}^{t_4} v_a(t)dt = \frac{2D\eta\omega\sigma U_r}{\pi f(\Delta_s - \Delta_{\min})} \left[\frac{\pi}{2} - \arcsin\left(1 - \frac{\Delta_s - \Delta_{\min}}{A}\right) \right] \quad (7)$$

2.3. Modelling of Composite Processing

In actual machining, the material removal is the superimposed effect of UAG and ultrasonic-assisted electrochemical action. Based on the two above-mentioned models, the material removal model for rotating ultrasonic compound electrochemical processing can be derived, and the material removal depth h_3 can be expressed by using the following equation:

$$h_3 = h_1 + h_2 \quad (8)$$

Taking Equations (3) and (7) into (8), the following equation is obtained:

$$h_3 = \frac{Nh^2\pi^2nR}{S\pi f} \left[\frac{\pi}{2} - \arcsin\left(1 - \frac{h}{A}\right) \right] \sqrt{2rh - h^2} + \frac{2D\eta\omega\sigma U_r}{\pi f(\Delta_s - \Delta_{\min})} \left[\frac{\pi}{2} - \arcsin\left(1 - \frac{\Delta_s - \Delta_{\min}}{A}\right) \right] \quad (9)$$

Combining the above-mentioned derived equations, the ultrasonic amplitude A , the spindle speed n and the radius r of the microfine abrasive grain will affect the UAG action. The grinding action will be enhanced when the spindle speed increases or the particle size becomes larger. The electrochemical effect can be improved by changing the electrochemical voltage U_r or the conductivity σ . The oscillation force and enhanced grinding effect will increase with ultrasonic amplitude. The model ignores the ultrasonic pumping effect on the electrolyte and the removal effect of ultrasonic cavitation on the passivation film; thus, the effect of ultrasonic amplitude A and frequency f on the processing is not fully reflected in the model, which needs to be further determined in experiments.

Based on the above-mentioned model, UAECG will increase the processing efficiency, and the MRR is related to the machining parameters such as electrochemical voltage. In verifying the above-mentioned theory, a series of experiments is conducted.

3. Experimental Setup and Methods

3.1. Equipment

On the basis of the above-mentioned principle, a processing test system is designed. As shown in Figure 3, the designed UAECG system consists of two parts. The first part is a processing system, which provides ultrasonic grinding power to achieve composite and UAG. The second part is online measurement and the control system, which achieves online measurement and real-time control of the processing parameters through laser displacement sensors and other components.

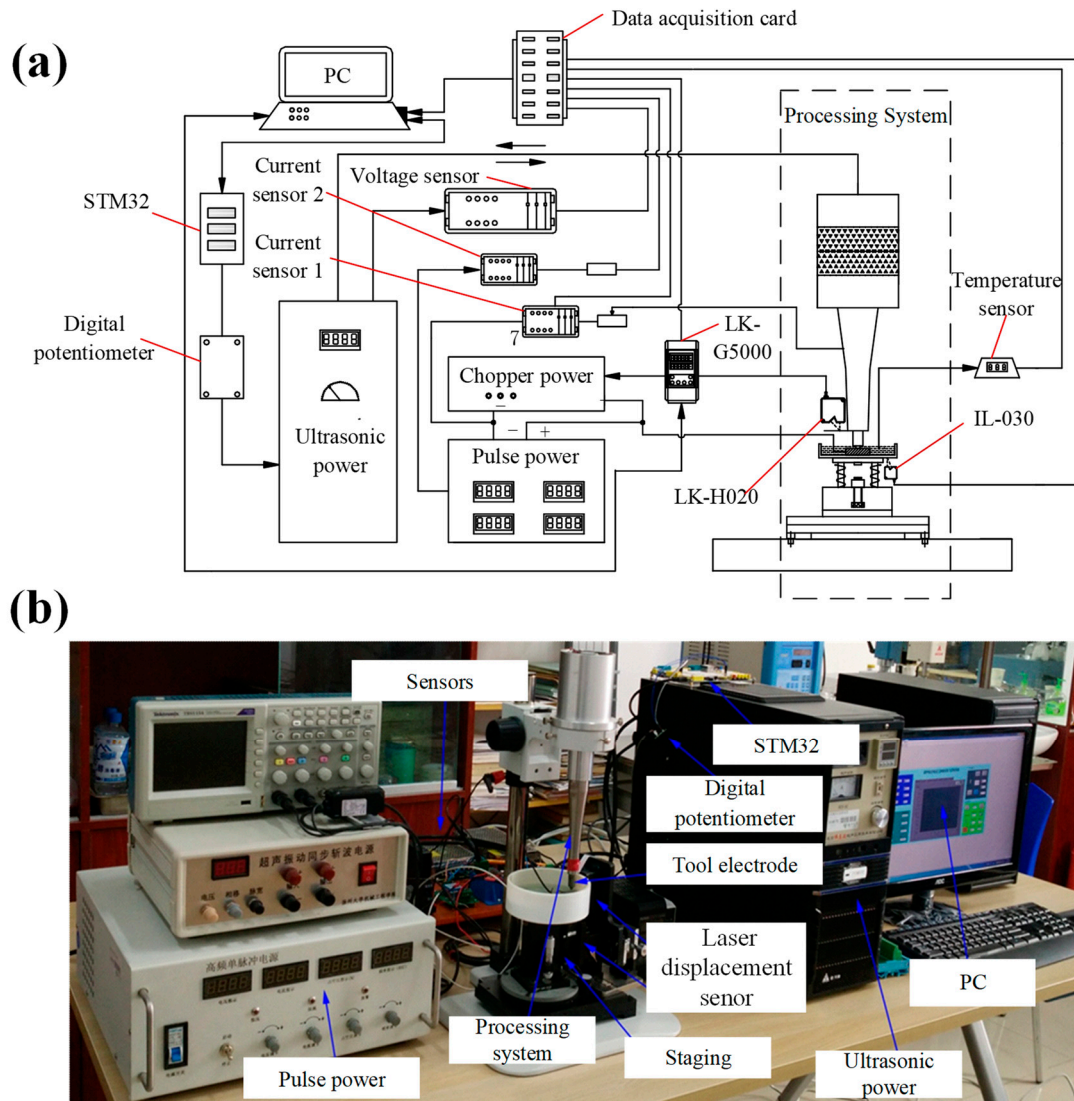


Figure 3. (a) Schematic diagram; (b) actual machining system.

3.2. Processing System

As shown in Figure 4, the processing system consists of a rotating ultrasonic spindle and an automatic feed system.

As shown in Figure 4a, the rotating ultrasonic spindle includes a rotating electrode, sandwich-type piezoelectric transducer, stepped ultrasonic variation rod and tool electrode. The tool electrode is covered with a diamond-solidified abrasive, and the substrate is a heat-treated high-strength tungsten-steel material, which can widely process hard, tough materials. The tool cathode and amplitude converter rod are connected by threads, which are coated with petroleum jelly to prevent energy loss during vibration [30].

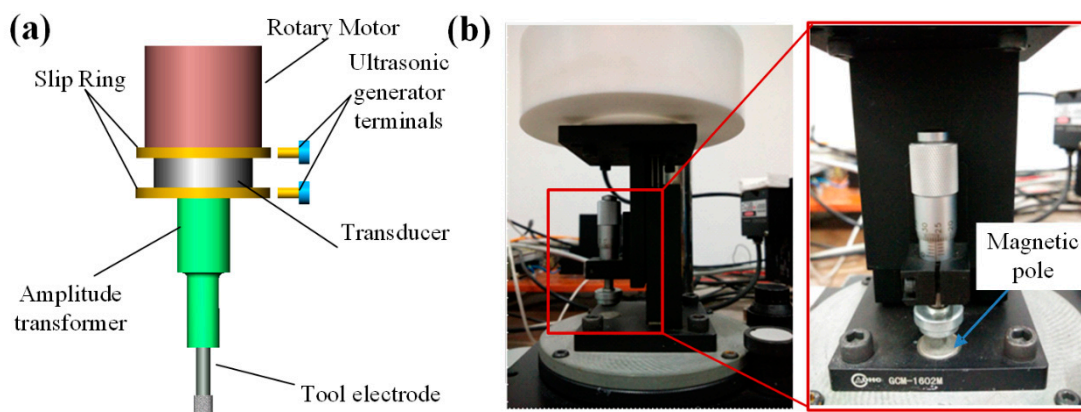


Figure 4. (a) Schematic diagram of the rotating ultrasonic spindle and (b) magnetic suspension table.

After connecting the ultrasonic power supply and spindle-rotating AC power supply, the ultrasonic spindle drives the ultrasonic amplitude rod and tool electrode in rotational grinding motion, whereas the transducer drives the amplitude rod and tool electrode for axial ultrasonic vibration. The ultrasonic spindle is avoided for rotation by adding a slip ring device. A fixed carbon brush is connected to the ultrasonic generator, which transmits the signal to the slip ring. Carbon brushes and the slip ring have a clearance to ensure that the slip ring rotates with the rotating electrode. The current passes through the ultrasonic generator to the carbon brush, then to the slip ring and the transducer, which ensures the synchronisation of motor rotation and ultrasonic axial motion.

As shown in Figure 4b, the automatic feed system is completed by the magnetic suspension table. Before processing, the workpiece is bonded to the workbench, and the workpiece moves in the X-axis and Y-axis directions by adjusting the X and Y knobs; thus, the cathode tool head reaches the upper part of the intended machining position on the workpiece. By adjusting the distance between the two magnetic poles on the spiral micrometre, the table maintains a certain height. During processing, the tool head and workpiece maintain a certain static pressure; the table in the magnetic pole's repulsive force increases with the increase in the depth of processing to ensure the continuous processing of the workpiece.

3.3. Online Measurement and Control System

As shown in Figure 2, the designed online measurement and control system are composed of a PC, microcontroller, digital potentiometer and different kinds of sensors. The LK-H020 laser-sensing head is used for the measurement of ultrasonic amplitudes. The LK-G5000 controller transmits the measurement data from LK-H020 to the PC via a serial port for data reading and setting. The displacement signal transmits to the computer via the USB interface. The IL-030 laser displacement sensor is used to detect the machining depth value. Two current sensors are designed to detect the inter-pole current and pulse power of machining. Current sensor 2 is connected to a rated resistor. The voltage sensor is used to measure the output voltage of the ultrasonic power supply. The temperature of the working fluid is detected by the temperature sensor. The above-mentioned sensors deliver the collected signals in analogue voltage to the data acquisition card, which is converted into digital signals by data acquisition and delivered to the PC. The microcontroller STM32 regulates the ultrasonic power supply voltage by controlling a digital potentiometer. Using the system, the processing parameters, such as ultrasonic amplitude, electrochemical voltage, electrochemical current and processing depth, are measured in real time. Thus, automatic control is performed to ensure that the process is in an envisioned stable state.

In achieving the above-mentioned synchronisation, a synchronous co-electrochemical device is designed (Figure 5). The displacement signal of the tool head vibration is connected to the chopper circuit, which is measured by using a laser micro displacement sensor. It is compared with the reference voltage signal set by the voltage comparator. On the

basis of the comparison result, the switching state of the photocoupler is decided, which generates the chopper pulse signal to control the MOS chopper tube switching. Whether the electrochemical power supply is turned on or turned off is determined by MOS. In this circuit, the current-continuity diode plays a role in protecting the MOS tube from being broken or burned by the induced voltage. The reference voltage of the voltage comparator can be changed by adjusting the value of resistor R3.

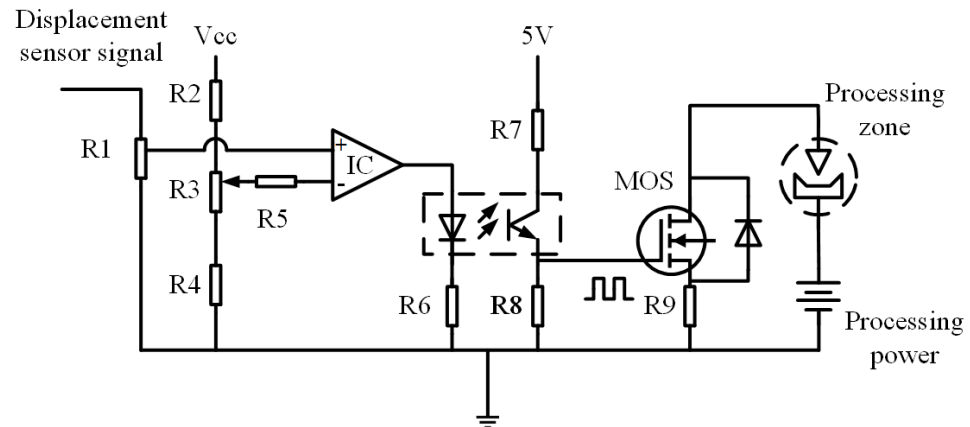


Figure 5. Synchronous processing control circuit.

3.4. Experimental Methods

In verifying the universality of the machining system for hard, tough materials, three hard, tough materials, namely, W18Cr4V, YT15 and SiCp/Al, were selected for three validation tests.

The performance of UAECG and UAG machining and UG machining for different machining efficiency and surface roughness for the same workpiece material (W18Cr4V) and machining process parameters was compared. Therefore, apart from the workpiece material, the machining method is another test factor.

Subsequently, considering that the electrolytic power supply has an important effect on the machining efficiency in the abovementioned model study, the electrolytic power supply was also used as a test variable parameter. In addition, previous UAECM studies have found a significant improvement in processing efficiency at a voltage variation range of 2–6 V [14]. In the UAECG designed in this paper, the relevant voltage parameter level settings are also considered, and the experimental situations are analysed at 2, 4 and 6 V.

Therefore, three factor levels of the processing effect, including the processing method, material and voltage, were studied and analysed, and the factor levels are listed in Table 1.

Table 1. Level of factors.

Level	Factors		
	Workpiece Material	Processing Methods	Voltage
−1	W18Cr4V	GM	2 V
0	YT15	UAG	4 V
1	SiCp/Al	UAECG	6 V

The electrolyte solution contained 5 wt.% NaNO₃. The spindle speed was set as 1000 r/min. The ultrasonic amplitude was set at 6 μm. The processing tests are presented in Table 2.

GM, UAG and UAECG were used for W18Cr4V machining tests to compare the influence of different processing methods on processing results. In acquiring the effect of machining voltage on the MRR, machining tests were conducted on YT15 using the UAECG system at different electrochemical voltages to investigate the effect of electrochemical

voltage on machining efficiency and accuracy. In addition, SiCp/Al is machined by using the UAECG system to study the impact of different voltages on surface morphology.

Table 2. Processing parameters.

NO	Workpiece Material	Processing Methods	Voltage
1	−1	−1	0
2	−1	0	0
3	−1	1	0
4	0	1	−1
5	0	1	0
6	0	1	1
7	1	1	−1
8	1	1	0
9	1	1	1

All tests lasted for 2 min. In minimising experimental errors, all tests were repeated three times, and the average value was taken as the test result. The size and microscopic shape of machined parts were acquired by using a stereo microscope, and the surface roughness was measured by using an interference microscope.

4. Results

4.1. Effect of Processing Methods

As shown in Figure 6a, the diameter and depth of the round hole machined by UAG are 1.7 times larger than those made by grinding. In addition, the depth of UAECG is 2.7 times higher than that of conventional grinding. Therefore, the MRR of the UAECG is higher than that of UAG and GM.

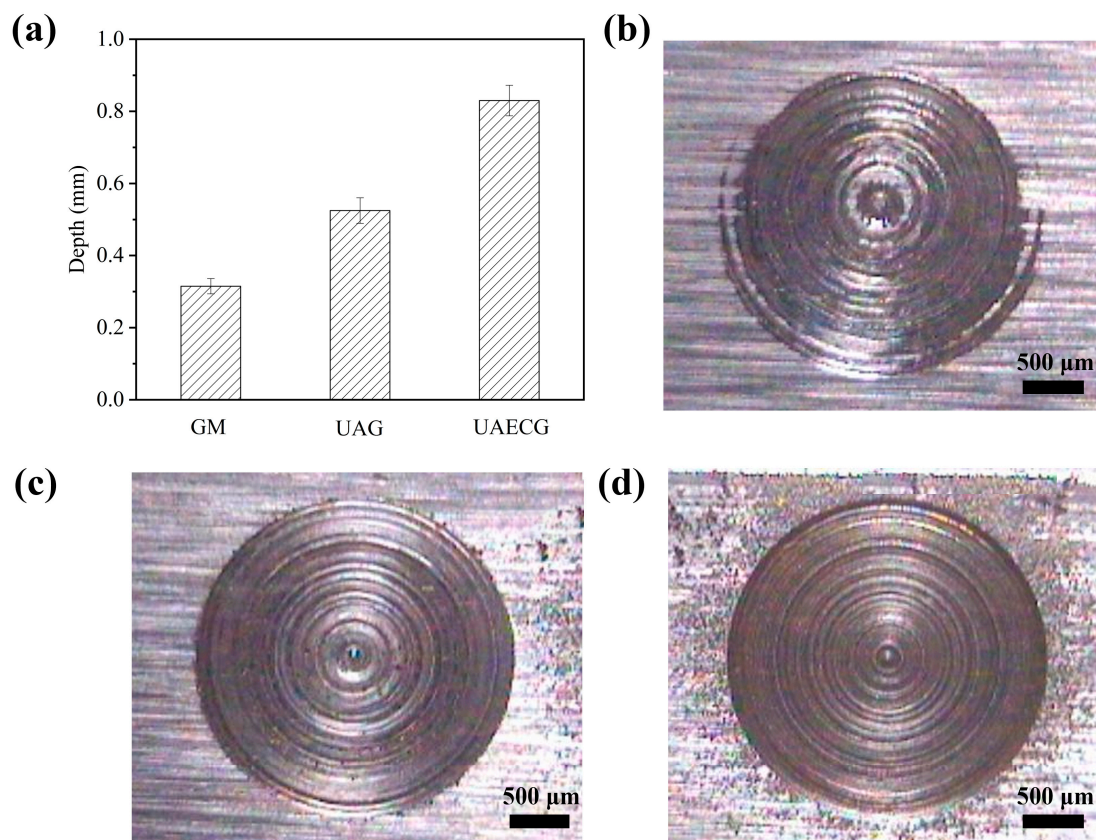


Figure 6. (a) Comparison of machining depth; (b) GM; (c) UAG; (d) UAECG.

As shown in Figure 6b,c, the hole achieved by the UAECG system is the deepest, and the hole surface is the smoothest. By contrast, the hole machined by conventional processing is rough, and the machining efficiency is low. The surface of the hole machined by UAG is better than that machined by GM but not as good as that machined by UAECG. However, the surface around the machining, which need not be machined, is mostly affected in the UAECG. Considerable pitting dissolution can be observed on its surface.

4.2. Effect of Voltage on Processing Rate

As shown in Figure 7a, at the same processing time, the machining depth and machining efficiency increase with the increase in voltage. The depth of the round hole at 6 V is 3.1 times deeper than that at 2 V and 1.8 times deeper than that at 4 V.

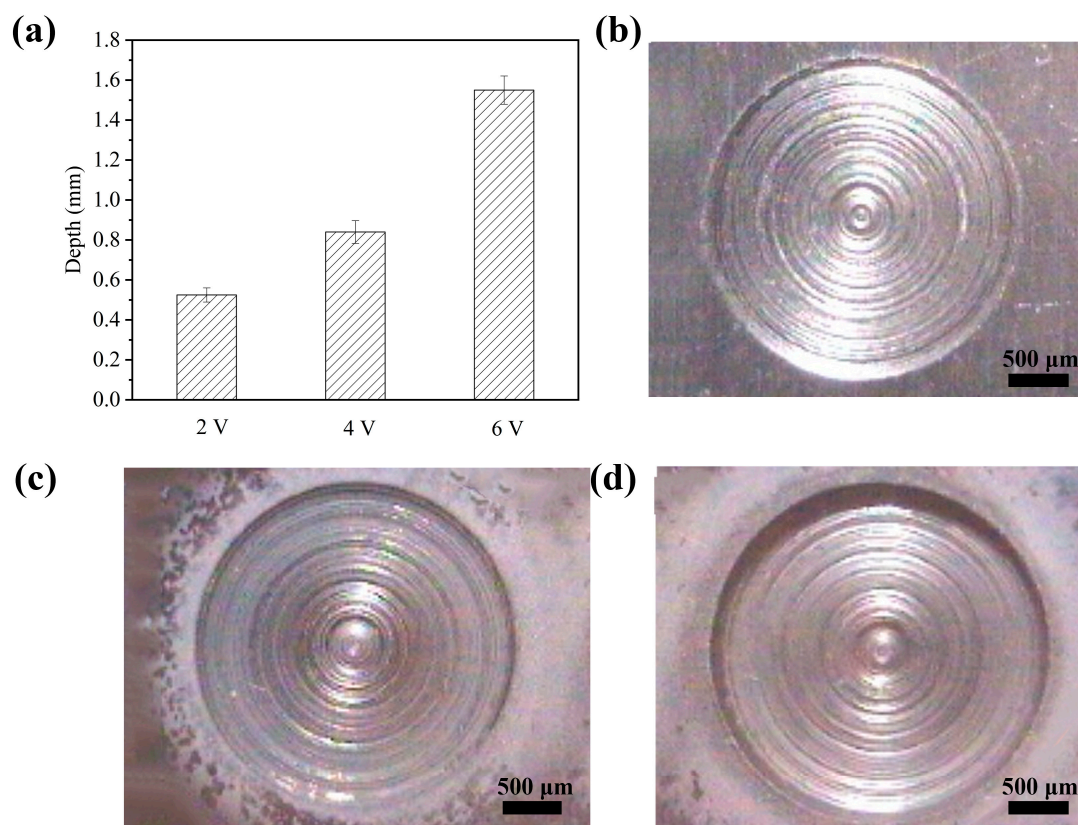


Figure 7. (a) Machining depth comparison; (b) 2 V machining shape; (c) 4 V machining shape; (d) 6 V machining shape.

As shown in Figure 7b–d, the depth of the hole at 6 V is the deepest one, and the hole at 2 V is the lowest one. In addition, the scratches caused by the abrasive grains on the end face of the tool electrode are evident at 2 V. Although the depth of the round hole is the largest, the roughness of the machined surface is not as good as the surface machined at 4 V.

4.3. Effect of Processing Voltage on Surface Morphology

As shown in Figure 8a, when the voltage increases from 2 to 4 V, the roughness of the workpiece surface decreases. However, when the voltage continues to increase to 6 V, the roughness begins to increase.

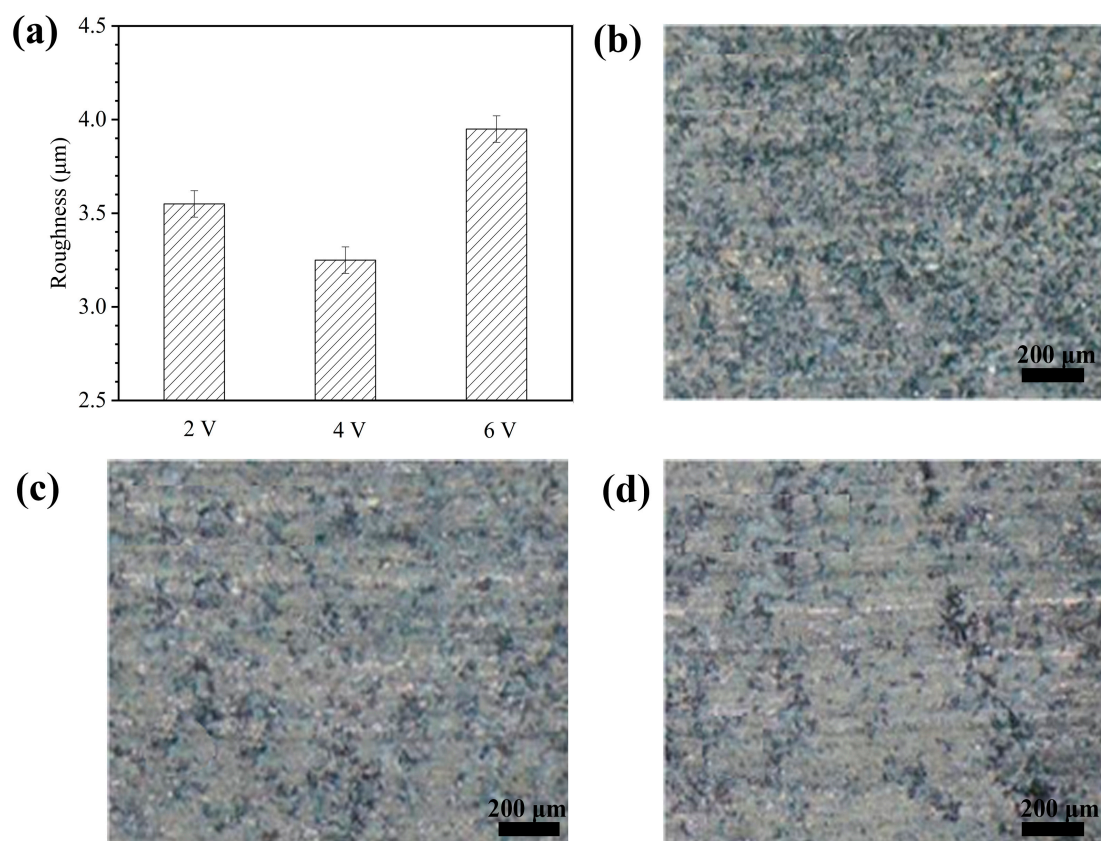


Figure 8. (a) Surface roughness comparison histogram; (b) microscopic surface shape at 2 V; (c) microscopic surface shape at 4 V; (d) microscopic surface shape at 6 V.

The same results can be observed in Figure 8b–d. The scratches caused by the abrasive grains on the end face of the tool electrode are evident at 2 V. When the electrochemical voltage increases to 4 V, the scratches are markedly reduced. However, when the voltage increases to 6 V, the stray corrosion becomes severe, and the machined surface quality decreases significantly.

5. Discussion

5.1. Effect of Processing Methods

The result indicates that the material removal efficiency improves with ultrasonic vibration-assisted grinding. Therefore, the quality is significantly better than the first two processing methods. However, considering the electrochemical machining factor, the surface around, which needs not to be machined, becomes rough.

Based on the above-mentioned experimental analysis, the following process laws can be obtained. UAECG couples mechanical energy, ultrasonic energy and electrical energy; thus, the processing efficiency and surface quality of W18Cr4V after processing can be improved by using this processing method. However, the surface around the hole will be affected more in this kind of machining.

5.2. Effect of Voltage on Processing Rate and Surface Morphology

The result indicates that the electrochemical effect is weak at 2 V, and the ultrasonic and grinding effects are dominant. Therefore, the surface morphology is good but the processing efficiency is the lowest. Subsequently, when the voltage grows to 4 V, the electrochemical effect and machining speed grow. Compared with the literature, the effect of voltage on processing is also comparable to that on UAECM. Therefore, voltage has a similar effect on the efficiency of UAECG processing.

However, at 6 V, the electrochemical effect tends to dominate the machining, thereby decreasing machining accuracy and surface quality. In this stage, the local point field strength and the formation of discharge channels will generate a micro-spark discharge when encountering difficult-to-machine bumps and small clearance. This phenomenon also affects the accuracy of the machined surface.

Based on the above-mentioned experimental analysis, the following process rules can be obtained: Changing the electrochemical voltage during machining can improve the machining efficiency. However, if the electrochemical voltage is excessively high, then partial discharge will occur when the clearance between the electrode and the workpiece of the ultrasonic tool is small to a certain extent. This phenomenon will affect the quality of the machined surface. Therefore, although the machining efficiency is improved by increasing the machining voltage, and the roughness has high requirements, a low voltage is necessary as the machining parameter to ensure the roughness meets the design requirements. Therefore, optimising the electrochemical voltage in the actual machining process is necessary.

6. Conclusions

An ultrasonic-assisted electrochemical grinding system was designed to improve the machining efficiency of hard, tough materials and to address the deficiency caused by conventional grinding, such as high machining temperatures and high tool losses. In this study, the mechanism of ultrasonic, electrochemical and grinding compound machining was investigated. Three materials were used as processing test objects, and a comparison of different forms and different parameters was performed to verify the extensive effectiveness during hard, tough material processing. The experimental and analytical results are presented as follows:

- (1) The machining efficiency of W18Cr4V can be improved by the UAECG system. The MRR is 2.7 times higher than that of conventional grinding and 1.7 times higher than UAG.
- (2) The ultrasonic amplitude, ultrasonic frequency, electrolyte conductivity and electrochemical voltage have a great influence on the processing. The processing efficiency increases with the increase in processing voltage, and the processing efficiency of YT15 is increased by 3.2 times when the processing voltage increased from 2 to 6 V.
- (3) The surface roughness of the SiCp/Al workpiece reached the best level at 4 V as the machining voltage increased from 2 to 6 V. The surface roughness increased significantly when the voltage increased to 6 V. Therefore, a comprehensive selection of parameters is necessary to increase processing efficiency under a satisfied surface roughness.
- (4) The combined use of ultrasonic energy, mechanical energy and electrolytic energy for UAECG processing is feasible, but a good set of processing parameters must be matched. In this paper, experimental studies were conducted on the variation of process parameters such as voltage, and further experiments on other parameters must be carried out in the future. Related research can provide a theoretical and practical basis for micro-hole machining of cemented carbide used in the aerospace and defence industry.

Author Contributions: Conceptualisation, C.H.; methodology, C.H.; validation, C.H.; formal analysis, C.H.; writing—original draft preparation, C.H.; writing—review and editing, Y.Z.; visualisation, Y.Z. All authors have read and agreed to the published version of the manuscript.

Funding: This project is supported by the National Natural Science Foundation of China (52175438, 51775484). The authors give cordial thanks to these funding organisations.

Data Availability Statement: The authors confirm that the data supporting the findings of this study are available within the article.

Conflicts of Interest: The authors declare no conflict of interest.

References

1. Yin, G.; Gong, Y.; Li, Y.; Song, J.; Zhou, Y. Modeling and evaluation in grinding of SiCp/Al composites with single diamond grain. *Int. J. Mech. Sci.* **2019**, *163*, 105137. [[CrossRef](#)]
2. Zhang, Q.; To, S.; Zhao, Q.; Guo, B. Surface generation mechanism of WC/Co and RB-SiC/Si composites under high spindle speed grinding (HSSG). *Int. J. Refract. Met. Hard Mater.* **2016**, *56*, 123–131. [[CrossRef](#)]
3. Chern, G.L. Study on mechanisms of burr formation and edge breakout near the exit of orthogonal cutting. *J. Mater. Process. Technol.* **2006**, *176*, 152–157. [[CrossRef](#)]
4. Zhan, H.; Zhao, W. EDMing turbopump blisks. *Aircr. Eng. Aerosp. Technol.* **2002**, *74*, 19–22. [[CrossRef](#)]
5. Agarwal, S. On the mechanism and mechanics of material removal in ultrasonic machining. *Int. J. Mach. Tools Manuf.* **2015**, *96*, 1–14. [[CrossRef](#)]
6. Kozak, J. Mathematical models for computer simulation of electrochemical machining processes. *J. Mater. Process. Technol.* **1998**, *76*, 170–175. [[CrossRef](#)]
7. Gao, T.; Zhang, X.; Li, C.; Zhang, Y.; Yang, M.; Jia, D.; Ji, H.; Zhao, Y.; Li, R.; Yao, P.; et al. Surface morphology evaluation of multi-angle 2D ultrasonic vibration integrated with nanofluid minimum quantity lubrication grinding. *J. Manuf. Process.* **2020**, *51*, 44–61. [[CrossRef](#)]
8. Jianhua, Z.; Hui, L.; Minglu, Z.; Yan, Z.; Liying, W. Study on force modeling considering size effect in ultrasonic-assisted micro-end grinding of silica glass and Al₂O₃ ceramic. *Int. J. Adv. Manuf. Technol.* **2017**, *89*, 1173–1192. [[CrossRef](#)]
9. Shen, X.H.; Shi, Y.L.; Zhang, J.H.; Zhang, Q.J.; Tao, G.C.; Bai, L.J. Effect of process parameters on micro-textured surface generation in feed direction vibration assisted milling. *Int. J. Mech. Sci.* **2019**, *167*, 105267. [[CrossRef](#)]
10. Li, Z.; Yuan, S.; Song, H.; Batako, A.D.L. A cutting force model based on kinematics analysis for C/SiC in rotary ultrasonic face machining. *Int. J. Adv. Manuf. Technol.* **2018**, *97*, 1223–1239. [[CrossRef](#)]
11. Wang, H.; Zhang, D.; Li, Y.; Cong, W. The effects of elliptical ultrasonic vibration in surface machining of CFRP composites using rotary ultrasonic machining. *Int. J. Adv. Manuf. Technol.* **2020**, *106*, 5527–5538. [[CrossRef](#)]
12. Zhang, X.; Yang, L.; Wang, Y.; Lin, B.; Dong, Y.; Shi, C. Mechanism study on ultrasonic vibration assisted face grinding of Hard and brittle materials. *J. Manuf. Process.* **2020**, *50*, 520–527. [[CrossRef](#)]
13. Bhattacharyya, B.; Malapati, M.; Munda, J.; Sarkar, A. Influence of tool vibration on machining performance in electrochemical micro-machining of copper. *Int. J. Mach. Tools Manuf.* **2007**, *47*, 335–342. [[CrossRef](#)]
14. Ghoshal, B.; Bhattacharyya, B. Influence of vibration on micro-tool fabrication by electrochemical machining. *Int. J. Mach. Tools Manuf.* **2013**, *64*, 49–59. [[CrossRef](#)]
15. Skoczypiec, S. Research on ultrasonically assisted electrochemical machining process. *Int. J. Adv. Manuf. Technol.* **2011**, *52*, 565–574. [[CrossRef](#)]
16. Wang, M.; Zhang, Y.; He, Z.; Peng, W. Deep micro-hole fabrication in EMM on stainless steel using disk micro-tool assisted by ultrasonic vibration. *J. Mater. Process. Technol.* **2016**, *229*, 475–483. [[CrossRef](#)]
17. Wang, Y.; Zeng, Y.; Zhang, W. Improving the machining efficiency of electrochemical micromachining with oscillating workpiece. *Int. J. Adv. Manuf. Technol.* **2019**, *102*, 2695–2708. [[CrossRef](#)]
18. Volgin, V.M.; Lyubimov, V.V.; Davydov, A.D. Modeling and numerical simulation of electrochemical micromachining. *Chem. Eng. Sci.* **2016**, *140*, 252–260. [[CrossRef](#)]
19. Singh, T.; Dvivedi, A. Developments in electrochemical discharge machining: A review on electrochemical discharge machining, process variants and their hybrid methods. *Int. J. Mach. Tools Manuf.* **2016**, *105*, 1–13. [[CrossRef](#)]
20. Pei, Z.J.; Ferreira, P.M. Experimental investigation of rotary ultrasonic face milling. *Int. J. Mach. Tools Manuf.* **1999**, *39*, 1327–1344. [[CrossRef](#)]
21. Pei, Z.J.; Ferreira, P.M. Modeling of ductile-mode material removal in rotary ultrasonic machining. *Int. J. Mach. Tools Manuf.* **1998**, *38*, 1399–1418. [[CrossRef](#)]
22. Li, C.; Zhang, F.; Meng, B.; Liu, L.; Rao, X. Material removal mechanism and grinding force modelling of ultrasonic vibration assisted grinding for SiC ceramics. *Ceram. Int.* **2017**, *43*, 2981–2993. [[CrossRef](#)]
23. Zhang, Y.; Li, C.; Ji, H.; Yang, X.; Yang, M.; Jia, D.; Zhang, X.; Li, R.; Wang, J. Analysis of grinding mechanics and improved predictive force model based on material-removal and plastic-stacking mechanisms. *Int. J. Mach. Tools Manuf.* **2017**, *122*, 81–97. [[CrossRef](#)]
24. Zhou, L.; Wang, Y.; Ma, Z.Y.; Yu, X.L. Finite element and experimental studies of the formation mechanism of edge defects during machining of SiCp/Al composites. *Int. J. Mach. Tools Manuf.* **2014**, *84*, 9–16. [[CrossRef](#)]
25. Zhao, B.; Chang, B.; Wang, X.; Bie, W. System design and experimental research on ultrasonic assisted elliptical vibration grinding of Nano-ZrO₂ ceramics. *Ceram. Int.* **2019**, *45*, 24865–24877. [[CrossRef](#)]
26. Arefin, S.; Zhang, X.Q.; Neo, D.W.K.; Kumar, A.S. Effects of cutting edge radius in vibration assisted micro machining. *Int. J. Mech. Sci.* **2021**, *208*, 106673. [[CrossRef](#)]
27. Wüthrich, R.; Fascio, V. Machining of non-conducting materials using electrochemical discharge phenomenon—An overview. *Int. J. Mach. Tools Manuf.* **2005**, *45*, 1095–1108. [[CrossRef](#)]
28. Zhang, X.; Arif, M.; Liu, K.; Kumar, A.S.; Rahman, M. A model to predict the critical undeformed chip thickness in vibration-assisted machining of brittle materials. *Int. J. Mach. Tools Manuf.* **2013**, *69*, 57–66. [[CrossRef](#)]

29. Hewidy, M.S.; Ebeid, S.J.; El-Taweel, T.A.; Youssef, A.H. Modelling the performance of ECM assisted by low frequency vibrations. *J. Mater. Process. Technol.* **2007**, *189*, 466–472. [[CrossRef](#)]
30. Zarepour, H.; Yeo, S.H. Predictive modeling of material removal modes in micro ultrasonic machining. *Int. J. Mach. Tools Manuf.* **2012**, *62*, 13–23. [[CrossRef](#)]

Disclaimer/Publisher’s Note: The statements, opinions and data contained in all publications are solely those of the individual author(s) and contributor(s) and not of MDPI and/or the editor(s). MDPI and/or the editor(s) disclaim responsibility for any injury to people or property resulting from any ideas, methods, instructions or products referred to in the content.